SCIENTIFIC REP♀RTS

OPEN

Electrocatalytic performances of g-C$_3$N$_4$-LaNiO$_3$ composite as bi-functional catalysts for lithium-oxygen batteries

Yixin Wu[1], Taohuan Wang[1], Yidie Zhang[1], Sen Xin[1], Xiaojun He[2], Dawei Zhang[1,3] & Jianglan Shui[4]

A low cost and non-precious metal composite material g-C$_3$N$_4$-LaNiO$_3$ (CNL) was synthesized as a bifunctional electrocatalyst for the air electrode of lithium-oxygen (Li-O$_2$) batteries. The composition strategy changed the electron structure of LaNiO$_3$ and g-C$_3$N$_4$, ensures high Ni^{3+}/Ni^{2+} ratio and more absorbed hydroxyl on the surface of CNL that can promote the oxygen reduction reaction (ORR) and oxygen evolution reaction (OER). The composite catalyst presents higher activities than the individual components g-C$_3$N$_4$ and LaNiO$_3$ for both ORR and OER. In non-aqueous Li-O$_2$ batteries, CNL shows higher capacity, lower overpotentials and better cycling stability than XC-72 carbon and LaNiO$_3$ catalysts. Our results suggest that CNL composite is a promising cathode catalyst for Li-O$_2$ batteries.

Li-O$_2$ battery is a promising energy storage solution, as it has a theoretical specific energy of 5200 Wh kg^{-1} (including O$_2$), much higher than the state-of-the-art Li-ion battery[1–3]. A typical non-aqueous Li-O$_2$ cell is composed of a piece of lithium metal as the anode, electrolyte and a piece of porous air electrode as the cathode. During the discharge reaction, the oxygen reduction reaction happens in the cathode producing lithium peroxides (Li$_2$O$_2$)[4]. During the charge, a reversal reaction of oxygen evolution reaction happens, decomposing Li$_2$O$_2$ to oxygen and Li-ions again[5]. It is crucial to utilize highly efficient catalysts to promote the ORR/OER process. So far, many metals, metal oxides, carbonaceous materials and redox media have been reported as cathode catalysts in Li-O$_2$ batteries[6–10]. The noble metal and noble metal oxide nanoparticles are usually the highly efficient catalyst, however, the high cost of the noble metals have limited their large-scale applications[11,12].

Graphitic carbon nitride (g-C$_3$N$_4$) polymer, has a planar phase analogous to graphite. Unlike graphite, however, g-C$_3$N$_4$ has both 3-fold-coordinated (graphite-like) and 2-fold-coordinated (pyridine-like) nitrogen atoms, and every carbon atom is bonded to three nitrogen atoms, including both pyridinic and graphitic nitrogen moieties[13]. g-C$_3$N$_4$ is an attractive catalysis material due to its properties like high chemical stability, low-cost preparation and specificity in the structure and composition[14]. So far, it has been used in many areas, such as the photochemical splitting of water, fuel cells, and metal-free heterogeneous catalysis of various organic reactions[15–20]. In particular, g-C$_3$N$_4$ contains alleged "nitrogen pots" with six nitrogen lone-pair electrons, which enable the material to modify the electronic structures of the molecular and to be ideal sites for metal inclusion[21,22]. However, the poor electroconductivity and the relatively low ORR catalytic activity limit the electrocatalytic application of g-C$_3$N$_4$[23]. These problems can be solved by compositing g-C$_3$N$_4$ with other materials which have better electrical conductivity. For example, g-C$_3$N$_4$ combined with non-noble metals like Co-g-C$_3$N$_4$[24], Fe-g-C$_3$N$_4$[25], and Ni-Co$_3$O$_4$-C$_3$N$_4$[26] have been investigated as the effective catalysts in fuel cells and Li-O$_2$ batteries. The composites have shown promising ORR and OER activity and tolerance ability that are comparable to commercial Pt/C.

Perovskite oxides (ABO$_3$) have been widely used as catalysts for fuel cells and metal-O$_2$ batteries[27], owing to their unique structures, excellent oxygen mobility and low cost. LaNiO$_3$ has the intrinsic activity for both ORR and OER among the perovskite type oxides, because Ni^{3+} at B site in the perovskite structure has single

[1]School of Chemistry and Chemical Engineering, Hefei University of Technology, Hefei, 230009, China. [2]School of Chemistry and Chemical Engineering, Anhui University of Technology, Maanshan, 243002, China. [3]CAS Key Laboratory of Materials for Energy Conversion, Hefei, 230026, China. [4]School of Materials Science and Engineering, Beihang University, Beijing, 100191, China. Correspondence and requests for materials should be addressed to D.Z. (email: zhangdw@ustc.edu.cn) or J.S. (email: shuijianglan@buaa.edu.cn)
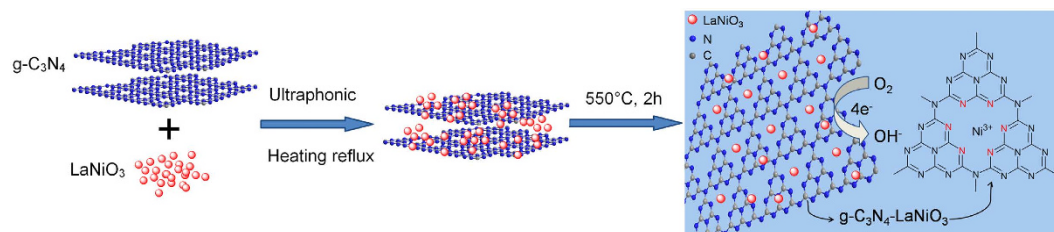
Figure 1. Schematic illustration of the synthetic process of CNL composite.
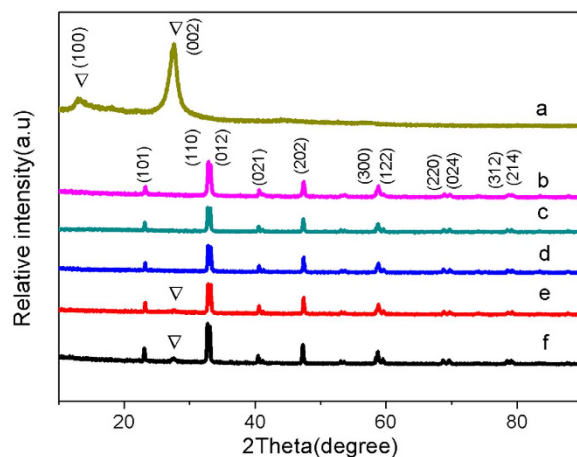
Figure 2. XRD patterns of (**a**) g-C$_3$N$_4$, (**b**) LaNiO$_3$, (**c**) 5 wt.% CNL, (**d**) 10 wt.% CNL, (**e**) 20 wt.% CNL, (**f**) 30 wt.% CNL hybrid catalyst. The weight percentage number imply the g-C$_3$N$_4$.

electron-filled e$_g$ orbit, and therefore, provides the favorable bond energy of M (B site)-O bond for ORR and OER[28]. In addition, the catalytic activity of LaNiO$_3$ could be readily enhanced through increasing the Ni^{3+}/Ni^{2+} ratio by replacing part of Ni ions with Mg or Fe ions. g-C$_3$N$_4$ has a large number of removable electronic between layers, and cavities encircling with some pyridine-like nitrogen[29]. So it has a high ability to complex with abundant metal ions and adjust its conjugation structure subsequently. Therefore combining g-C$_3$N$_4$ with LaNiO$_3$ can theoretically improve the electron transfer and catalytic activity of the CNL composite. However, to the best of our knowledge, g-C$_3$N$_4$ have never been composited with LaNiO$_3$ to explore the enhanced the catalytic activity for both ORR and OER.

In this work, we synthesized a composite catalyst g-C$_3$N$_4$-LaNiO$_3$ (CNL), and demonstrated that the CNL has significantly enhanced electrocatalytic activity for OER and ORR compared with individual component g-C$_3$N$_4$ or LaNiO$_3$ in an alkaline electrolyte. Furthermore, CNL exhibited improved round-trip efficiency and cycling stability in Li-O$_2$ batteries. These results suggest that the CNL is a promising bi-functional catalyst for oxygen oxidation/evolution reactions.

Results and Discussion

Characterization of CNL catalyst.
Figure 1 depicts the synthetic process of CNL catalyst and the molecular structure of the catalytic spots of CNL catalyst. Figure 2 displays the XRD patterns of pure g-C$_3$N$_4$, LaNiO$_3$ and the hybrid catalyst CNL with different weight percent of g-C$_3$N$_4$. It can be seen that the pure g-C$_3$N$_4$ has two distinct peaks. The strong peak at 27.39°, corresponding to the (002) peak with in-planar distance of 0.326 nm (JCPDS 87–1526), is attributed to the long-range in-planar stacking of aromatic units[30]. Another peak at 13.08°, with a much weaker intensity, can be assigned to (100) diffraction peak[20], which corresponds to a distance of 0.686 nm, belongs to tri-s-triazine units, due to the interlayer stacking. After the LaNiO$_3$ being composited with g-C$_3$N$_4$, the CNL hybrids show a coexistence phases of both g-C$_3$N$_4$ and LaNiO$_3$, although the characteristic peak of g-C$_3$N$_4$ was not obvious for the 5 wt.% and 10 wt.% CNL hybrids.

For the further information of the materials microstructure, Fig. 3 shows the SEM images of g-C$_3$N$_4$, LaNiO$_3$ and 10 wt.% CNL. Pure g-C$_3$N$_4$ shows an aggregated layered structure with smooth surface. The agglomerate size is several micron meters. LaNiO$_3$ particles are hundreds nanometers large, more than one order of magnitude smaller than g-C$_3$N$_4$. As to the image of 10 wt.% CNL, LaNiO$_3$ particles are deposited on the surface of g-C$_3$N$_4$.

In this study we used the X-ray photoelectron spectra to research the physical and chemical characteristic of the composite catalyst surface. Figure 4a shows the O 1s XP-spectra of g-C$_3$N$_4$, LaNiO$_3$ and CNL catalysts. The O 1s XP-spectra contains four distinct species. Two low binding energy peaks located at 528.6 eV and 530.1 eV are ascribed to the lattice oxygen, O^{2-} species in lanthanum oxide and nickel oxide[31]. The peaks located at 531.5 eV and 532.2 eV are from lanthanum and nickel hydroxides[32,33]. With the increase of g-C$_3$N$_4$, the peaks
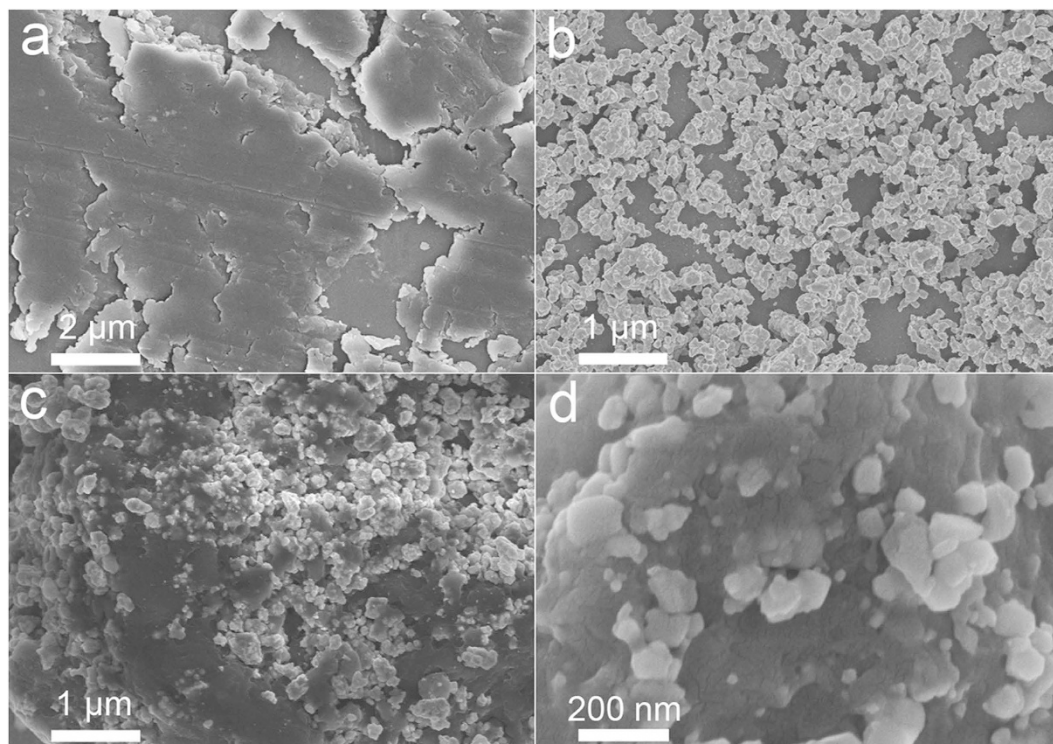
Figure 3. FE-SEM images of (**a**) g-C$_3$N$_4$, (**b**) LaNiO$_3$, (**c**) 10 wt.% CNL and (**d**) magnified images of 10 wt.% CNL hybrid catalyst.
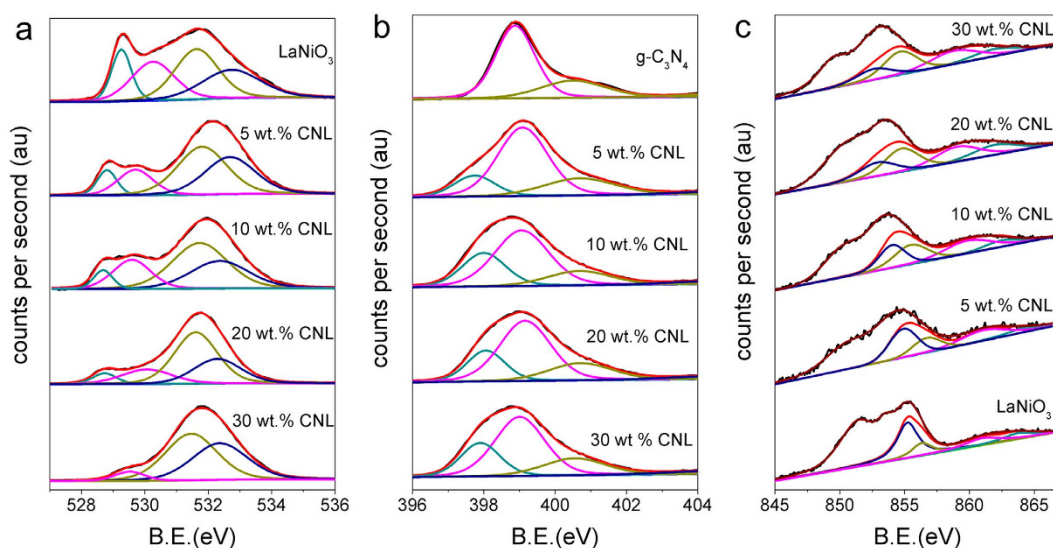
Figure 4. (**a**) O 1s XPS spectra, (**b**) N 1s XPS spectra and (**c**) Ni 2p$^{3/2}$ XPS spectra of LaNiO$_3$ and x wt.% CNL (x = 5, 10, 20 and 30) composite catalysts.

at low binding energy become weaken, and the peaks at high binding energy become stronger, indicating that the g-C$_3$N$_4$ compositing LaNiO$_3$ can promote the adsorption of hydroxyl on the surface of the composite catalyst and the covalency of Ni-O bond become stronger[34]. It has been demonstrated that the rate of O$_2^{2-}$/OH$^-$ displacement and OH$^-$ regeneration dominate the ORR kinetics, and the great covalence of the Ni-O bond can promote the ORR kinetics[30]. Furthermore, OER is either through chemisorbed OOH$^-$ formation or oxidation of surface OH$^-$. The rate-determining step of the OER on perovskite oxides is governed by the concentration of hydroxide species that participate in the formation of the O-O bond in hydroperoxide. Thus, the high lattice hydroxide concentration on the surface can promote the HOO$^-$ forms, and consequently has a positive effect on OER activity.
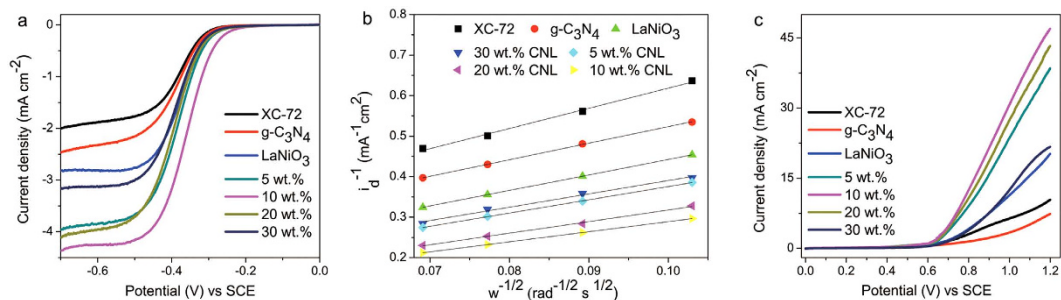
Figure 5. (**a**) ORR polarization curves, (**b**) Koutecky-Levich plots and (**c**) OER polarization curves of XC-72, g-C$_3$N$_4$, LaNiO$_3$ and x wt.% CNL (x = 5, 10, 20 and 30) catalysts.

The N 1s XPS spectrum of the g-C$_3$N$_4$ shown in Fig. 4b can be fitted into three peaks at 398.8, 400.5 and 404.7 eV, corresponding to pyridine-like N, pyrrole-like N, and oxidized N, respectively[35,36]. After adding g-C$_3$N$_4$, a new peak emerged at 398.2 eV, which also corresponds to pyridine-like N. The reason why it was lower than 398.8 eV, can be explained by the existence of chemical bonds in the g-C$_3$N$_4$-LaNiO$_3$ heterojunction.

Ni 2p$^{3/2}$ was deconvoluted into two peaks. The binding energy of 854.3 eV was due to Ni^{2+}, and 856 eV was due to Ni^{3+} as shown in Fig. 4c [31]. The peak intensity of the lower oxidation state (Ni^{2+}) is weakening and the higher oxidation state (Ni^{3+}) is enhancing with the increase of g-C$_3$N$_4$ in the composite. It suggests that through heat treating LaNiO$_3$ could be doped with nitrogen-atoms forming LaNiO$_{3-x}$N$_x$, which promoted the formation of Ni^{3+} on the surface of the composite catalyst. According to previous report, the existence of Ni^{3+} in LaNiO$_3$ are beneficial to both ORR and OER activities of the material[37].

Electrocatalytic performance. The typical polarization curves for the ORR was investigated in O$_2$ saturated 0.1 M KOH solution, shown in Fig. 5a. The ORR onset potential of 10 wt.% CNL is about −0.286 V, the most positive among that of LaNiO$_3$ (−0.304 V), 20 wt.% CNL (−0.319 V), 30 wt.% CNL (−0.315 V), g-C$_3$N$_4$ (−0.315 V) and XC-72 (−0.314 V). And the half-wave potential of 10 wt.% CNL is −0.35 V, ~350 mV higher than the 2nd high value of 5 wt.% CNL. In additional that the 10 wt.% CNL also exhibits the largest diffusion-limiting current, and the limiting current was 4.36 mA cm^{-2}, much higher than 2.82 mA cm^{-2} of LaNiO$_3$. Furthermore, for kinetic analysis the current-potential curves at various rotation speeds were also analyzed with the Koutecky-Levich equation:

$$\frac{1}{i_d} = \frac{1}{i_k} + \frac{1}{i_{dl}} \tag{1}$$

$$i_k = nFAkC_O \tag{2}$$

$$i_{dl} = B\omega^{\frac{1}{2}} = 0.62nFD_O^{\frac{2}{3}}\nu^{-\frac{1}{6}}C_O\omega^{\frac{1}{2}} \tag{3}$$

$$Slope = \frac{1}{Bn} \tag{4}$$

This equation has been widely used to analyze the ORR reaction kinetics[38–40], where i_d is the tested disk current-density, n is the number of electron transfer in the ORR, k is the Boltzmann constant, F is the Faraday constant, A is the geometric area of the disk electrode, C_O is the saturated concentration of oxygen in 0.1 M KOH solution, D_O is the diffusion coefficient of oxygen, ν is the kinematic viscosity of the 0.1 M KOH solution and ω is the electrode rotation rate. There should be a linear relationship between i_d^{-1} and $\omega^{-1/2}$, the intercept is equal to i_k^{-1}, and n could be calculated from the slope.

Figure 5b shows the Koutecky-Levich plots of XC-72, g-C$_3$N$_4$ and CNLs based on ORR polarization curves at −0.6 V with rotation speed of 2000, 1600, 1200 and 900 rpm. All curves exhibit good linear characteristic, indicating the first-order kinetics characteristics of the ORR. According to equations (3 and 4), the n value could be calculated as shown in Table 1. The n value of 10 wt.% CNL is about 3.86, indicating the ORR was a four-electrons process. In comparison with LaNiO$_3$ catalyst, as-synthesized 10 wt.% CNL material delivers a better ORR activity and kinetics. The higher electrocatalytic activity is due to the high Ni^{3+}/Ni^{2+} ratio in 10 wt.% CNL, which could promote adsorption/desorption of oxygen and thus the ORR activity in an alkaline electrolyte. Therefore in this work, the composite strategy has demonstrated to be highly effective to improve the ORR catalytic activity of the components.

The catalytic activity of the synthesized CNL for OER was also investigated by the RDE technique by measuring the polarization curves in O$_2$ saturated 0.1 M KOH solution from 0.0 V to 1.2 V, at a scan rate of 5 mV s^{-1} and a rotation speed of 1600 rpm. As shown in Fig. 5c, all the synthesized composite catalysts exhibit much better catalytic activity for OER than XC-72 carbon and LaNiO$_3$. The OER onset potential for LaNiO$_3$ is 0.70 V and the OER diffusion-limiting current density at 1.2 V is 20.2 mA cm^{-2}. For a comparison, the 10 wt.% CNL has a more

Sample	Slope	n	Intercept
XC-72	4.98294	2.006847	0.12019
g-C$_3$N$_4$	4.08943	2.445329	0.11453
LaNiO$_3$	3.82595	2.61373	0.05988
30 wt.% CNL	3.29416	3.035675	0.06098
5 wt.% CNL	3.26957	3.058506	0.04855
20 wt.% CNL	2.86083	3.495489	0.03153
10 wt.% CNL	2.58987	3.861198	0.02213

Table 1. Koutecky-Levich reasults of XC-72 Carbon, LaNiO$_3$ and x wt.% CNL (x = 0, 5, 10, 20 and 30) catalysts.
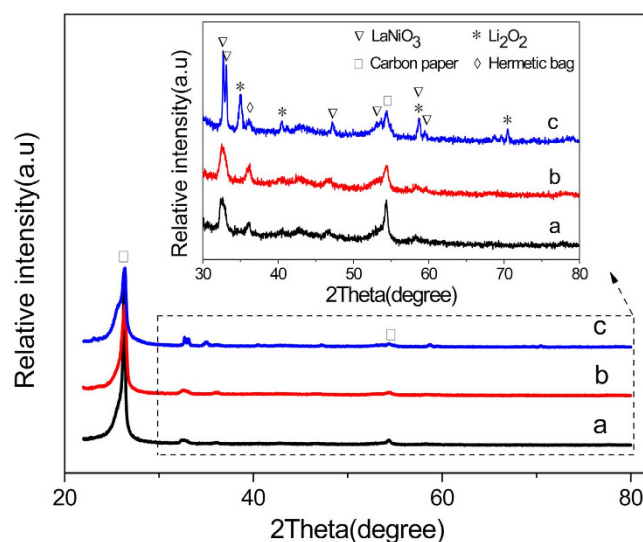

Figure 6. XRD patterns of the 10 wt.% CNL cathode for Li-O$_2$ batteries at (**a**) pristine, (**b**) 1st charged and (**c**) 1st discharged condition (In order to prevent the Li$_2$O$_2$ decomposition under the influence of water in the air, so put the cathode in a hermetic bag for XRD testing).

negative onset potential of 0.63 V, and the current density is 47.0 mA cm^{-2} at 1.2 V remarkably higher than that of LaNiO$_3$.

This improved property of 10 wt.% CNL is mainly due to the enhanced adsorption of hydroxyl on the surface of CNL composite. The hydroxyl participates in the formation of HOO$^-$, and the increase of the HOO$^-$ concentration leads to the high OER electrocatalytic activity. As to the elexctrocatalytic activity of g-C$_3$N$_4$, due to the stronger electro-negativity of N than C, the electron will transfer from C to adjacent N, while the π-conjugation causes the electrons to return to the adjacent Cp^2 orbital[41,42]. These donation and back-donation processes not only help the O^{2-} adsorption by the strong chemical bond between O and C, but also promote O$_2$ desorption on the adjacent C atoms, resulting in enhanced ORR and OER activity. The reason that ORR and OER activities of the 20 wt.% CNL and 30 wt.% CNL are lower than these of 10 wt.% CNL, can be interpreted by the worsen electron conductive environment due to too much non-conductive in the composites.

XRD was used to confirm the formation and decomposition of Li$_2$O$_2$ on the 10 wt.% CNL cathode during the charge-discharge process in non-aqueous Li-O$_2$ batteries. Figure 6 shows XRD patterns of the 10 wt.% CNL cathode at pristine,1st discharge and 1st recharge condition. After 1st discharge, compared to the XRD pattern of the pristine cathode, some diffraction peaks at 34.7, 40.3, 58.3 and 70.5° appear, which can be ascribed to Li$_2$O$_2$ formation during the discharging process. After the 1st charge process, the diffraction peaks of Li$_2$O$_2$ disappear, indicating that the formed Li$_2$O$_2$ in the 1st discharge is decomposed during the charging process. This XRD pattern evolution demonstrates the rechargeability of this 10 wt.% CNL cathode.

We further investigated the catalyst activity of the composites in non-aqueous Li-O$_2$ batteries. The first discharge and charge profiles of XC-72, LaNiO$_3$ and 10 wt.% CNL in the Li-air batteries were compared at a current density of 50 mA g^{-1} (Fig. 7a). In particular, the initial discharge capacity of the 10 wt.% CNL is 5500 mAh g^{-1}, higher than that of LaNiO$_3$ (4600 mAh g^{-1}) and XC-72 carbon (3600 mAh g^{-1}). Also, it can be clearly seen that the discharge voltage plateau of the 10 wt.% CNL catalyst was ~2.8 V, higher than that of the LaNiO$_3$ (~2.7 V) and the XC-72 carbon (~2.7 V). The charge voltage plateau of the 10 wt.% CNL was ~4.0 V, lower than that of LaNiO$_3$ (~4.3 V) and XC-72 carbon (~4.4 V). The smaller overvoltages of CNL suggests the higher catalytic activity than LaNiO$_3$ and XC-72. In additional, 10 wt.% CNL catalyst presented 65 cycles between voltage window of 2.6 V to 4.7 V as shown in Fig. 7b. While the performance of the LaNiO$_3$ and XC-72 carbon catalyst are only up to 32 and
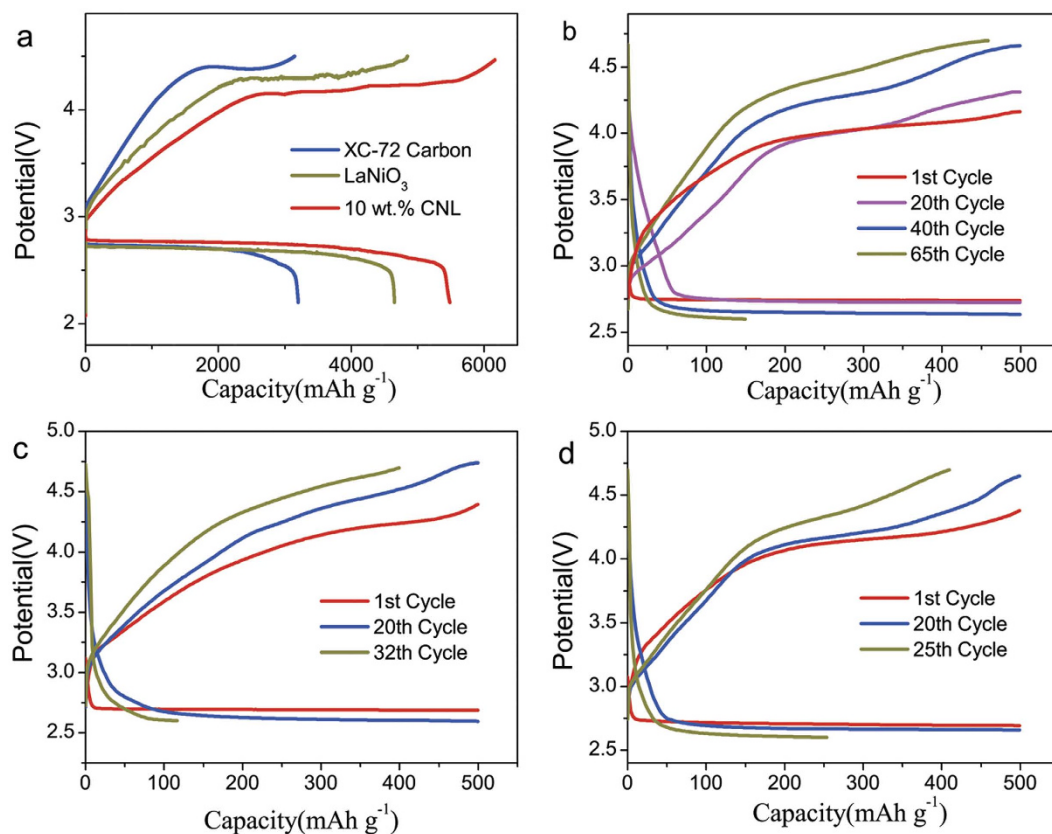
Figure 7. Electrochemical performances of Li-air batteries. (a) The first charge/discharge curve of Li-air batteries using XC-72 carbon, $LaNiO_3$ and 10 wt.% CNL as the air electrode at a current density of $50\,mA\,g^{-1}$. **(b–d)** Discharge and charge curve of the cells at a current density of $250\,mA\,g^{-1}$ using 10 wt.% CNL, $LaNiO_3$ and XC-72 carbon as the air electrode, respectively.

25 cycles respectively. These results indicate that the 10 wt.% CNL as air electrode catalyst enhanced the capacity and cyclability of $Li-O_2$ batteries.

In conclusion, $LaNiO_3$ and $g-C_3N_4$ composite was made as the bi-functional catalyst for oxygen reactions. The composite material delivers batter ORR and OER activities than individual $LaNiO_3$ and $g-C_3N_4$, the reason is that the CNL catalyst has a high Ni^{3+}/Ni^{2+} ratio that can promote adsorption/desorption of oxygen in an alkaline electrolyte, and more absorbed hydroxyl on the surface of CNL that can promote HOO^- formation. $LaNiO_3$ and $g-C_3N_4$ composite is for the first time used as the bi-functional catalysts for lithium air batteries. The composite presents enhanced specific capacity and cycle stability. The results suggest CNL composite can be a potential bifunctional catalyst for the $Li-O_2$ batteries, and the composite strategy is worth of further investigation.

Methods

Synthesis of $LaNiO_3$ NPs and $g-C_3N_4$ sheets. $LaNiO_3$ nanoparticles (NPs) were synthesized by a sol-gel method. $1.3\,g\,La_2O_3$ (Sinopharm, reagent grade) was dissolved in $10\,mL\,HNO_3$ solution ($65\% \leq HNO_3 \leq 68\%$), obtaining the $La(NO_3)_3 \cdot xH_2O$ solution. Then $2.37\,g\,Ni(NO_3)_2 \cdot 6H_2O$ (Sinopharm, reagent grade) and the $La(NO_3)_3 \cdot xH_2O$ were dissolved in $100\,ml$ de-ion water. Subsequently, the mixture of $6.75\,g$ citric acid ($HOC(COOH)(CH_2COOH)_2 \geq 99.5\%$) and $3.6\,mL$ ethylene glycol ($HOCH_2-CH_2OH$, 99.8%) were dropwise added into the metal nitrates under magnetic stirring at $80\,°C$. The molar ratios of total metal cations: citric acid: ethylene glycol were 1:2:4. Then the resulting solution was stirred at $80\,°C$ to evaporate water forming a viscous gel. The gel was heated at $400\,°C$ for 1 hour, and the amorphous citrate precursor was obtained. The precursor was milled and then calcinated in oxygen atmosphere at $750\,°C$ for 5 hours to obtain final $LaNiO_3$ powders.

Bulk $g-C_3N_4$ sheets were synthesized by pyrolysis method. Briefly, $5\,g$ melamine were heated at $550\,°C$ for 2 hours with a heating rate of $5\,°C\,min^{-1}$. The resultant agglomerates were ground for 1 hour in a mortar, then further heated at $550\,°C$ for 2 hours. Then the as-prepared bulk $g-C_3N_4$ were obtained.

Synthesis of CNL composite material. The CNL were synthesized as follows: $0.04\,g\,g-C_3N_4$ were dispersed in $50\,mL$ ethanol in a beaker, and treated by ultrasonic for 30 min to fully disperse $g-C_3N_4$. Then $0.4\,g$ $LaNiO_3$ NPs were added into the $g-C_3N_4$ suspension, and the mixture were further dispersed by the ultrasonic treatment for 30 min, and then heated under reflux for 6 hours at $90\,°C$ with stirring. Then evaporated the alcohol completely with stirring, a precipite was obtained. The precipitate was collected and heated at $550\,°C$ for 2 hours in nitrogen atmosphere. Then the resultant compound were ground for 1 hour in the mortar, to make the final

10 wt.% CNL composite material (the weight percentage number imply the g-C$_3$N$_4$). By this method, CNL catalysts in different mass ratios (5 wt.% CNL, 20 wt.% CNL and 30 wt.% CNL) were also prepared.

Characterization of materials. The crystal phase and purity of the as-prepared powders were determined by X-ray powder diffraction with Cu Kα radiation ($\lambda = 0.154056$ nm) from 10° to 90°. The structures of the samples were determined by field-emission scanning electron microscope (SEM) performed on a Hitachi SU8020 at an acceleration voltage of 3 kV. X-ray photoelectron spectra (XPS) data were obtained on a Rigaku D/MAX2500V X-ray photoelectron spectrometer with an exciting source of Al Kα (1486.6 eV).

Electrochemical measurements. Electrochemical characterizations of the samples were performed on a rotating-disk electrode (RDE, ATA-1B) with a three-electrode cell. A platinum electrode was used as the counter electrode. A saturated calomel electrode was used as the reference electrode. A glassy carbon electrode was used as the working electrode. 0.1 M potassium hydroxide (KOH) solution was used as the electrolyte. For CV, ORR and OER studies, the 1 mg composite catalyst powder was mixed with 2.5 mg XC-72 carbon to ensure sufficient electronic conductivity. The as-prepared catalyst and 30 μL of 5 wt.% Nafion solutions were dispersed in 1 mL de-ion water/isopropanol solution (the volume ratio of de-ion water: isopropanol is 5:1), with an ultrasonic treatment for 40 min to make a homogeneous ink. The glassy carbon electrodes (3 mm diameter, 0.071 cm^2 area) were polished on a clean polishing cloth with the 0.05 μm alumina slurry, rinsed and dried. Then we pipeted 2.8 μL of the suspension drop-cast and loaded it on the glassy carbon, which was dried slowly inside a closed container. The glassy carbon electrode loaded with catalyst was immersed into a N$_2$-saturated KOH electrolyte for the steady-state CVs. The N$_2$ was switched to O$_2$ and purged for another 30 min. After that the ORR polarization curve was measured from 0 V to -1.0 V. Then, switched the O$_2$ to N$_2$ and purged for 30 min. Subsequently, the OER polarization curve were examined by a voltage scan from 0.0 V to 1.2 V. Electrochemical data were collected with an Autolab electrochemical workstation.

For Li-O$_2$ battery studies, the battery were fabricated in a glove box which was filled with pure argon gas. A lithium foil was used as the anode, 1 M LiCF$_3$SO$_3$ in tetraethylene glycol dimethyl ether (TEGDME) as the electrolyte, glass fiber filter paper as separator, carbon-paper-supported catalysts as the cathode electrode and two piece of nickel foam (1 mm thick) as the cathode current collector[43,44]. The oxygen electrodes were prepared by mixing the as-prepared CNL catalysts, XC-72 carbon, 5 wt.% polyvinylidene fluoride (PVDF) and solvent N-methyl-2-pyrrolidone (NMP), and the mass ratio of CNL catalyst: XC-72 carbon: 5 wt.% PVDF is 1:2:3. The uniform slurry was coated onto the carbon-paper by a brush and dried in vacuum at 80 °C for 12 hours. The ready-made Li-O$_2$ battery were transferred into a sealed bottle which was filled with pure oxygen and linked with the multichannel battery testing system (LAND CT 2001A). Galvanostatic discharge of the battery were studied in a potential range of 4.5–2.0 V. The first discharge cycle performances were conducted at the current density of 50 mA g^{-1}. The following cycle performances were conducted at the current density of 250 mA g^{-1}, and the capacity was limited to 500 mAh g^{-1}. It should be noted that the current density and capacity were all calculated based on the mass of catalyst loaded on the cathode.

References

1. Abraham, K. M. & Jiang, Z. A polymer electrolyte-based rechargeable lithium/oxygen battery. *J. Electrochem. Soc.* **143,** 1–5 (1996).
2. Liu, T. *et al.* Cycling Li-O$_2$ batteries via LiOH formation and decomposition. *Science* **350,** 530–533 (2015).
3. Xu, J. J., Wang, Z. L., Xu, D., Zhang, L. L. & Zhang, X. B. Tailoring deposition and morphology of discharge products towards high-rate and long-life lithium-oxygen batteries. *Nat. Commun.* **4,** 2438 (2013).
4. Shui, J. L. *et al.* Reversibility of anodic Lithium in rechargeable Lithium-oxygen batteries. *Nat. Commun.* **4,** 1161–1171 (2013).
5. Liu, Q. C., Xu, J. J., Xu, D. & Zhang, X. B. Flexible lithium-oxygen battery based on a recoverable cathode. *Nat. Commun.* **6,** 7892 (2015).
6. Shui, J. L., Karan, N. K., Balasubramanian, M., Li, S. Y. & Liu, D. J. Fe/N/C composite in Li-O$_2$ battery: studies of catalytic structure and activity toward oxygen evolution reaction. *J. Am. Chem. Soc.* **134,** 16654–16661 (2012).
7. Rao, C. V., Cabrera, C. R. & Ishikawa, Y. In search of the active site in nitrogen-doped carbon nanotube electrodes for the oxygen reduction reaction. *J. Phys. Chem. Lett.* **1,** 2622–2627 (2010).
8. Nam, G. *et al.* Metal-free Ketjenblack incorporated nitrogen-doped carbon sheets derived from gelatin as oxygen reduction catalysts. *Nano lett.* **14,** 1870–1876 (2014).
9. Kwon, K., Sa, Y. J., Cheon, J. Y. & Joo, S. H. Ordered mesoporous carbon nitrides with graphitic frameworks as metal-free, highly durable, methanol-tolerant oxygen reduction catalysts in an acidic medium. *Langmuir* **28,** 991–996 (2011).
10. Oh, M. Y., Jeon, J. S., Lee, J. J., Kim, P. & Nahm, K. S. The bifunctional electrocatalytic activity of perovskite La$_{0.6}$Sr$_{0.4}$CoO$_{3-\delta}$ for oxygen reduction and evolution reactions. *RSC Adv.* **5,** 19190–19198 (2015).
11. Yang, Y., Shi, M., Zhou, Q. F., Li, Y. S. & Fu, Z. W. Platinum nanoparticle-graphene hybrids synthesized by liquid phase pulsed laser ablation as cathode catalysts for Li-air batteries. *Electrochem. Commun.* **20,** 11–14 (2012).
12. Li, H. *et al.* Nitrogen-doped carbon nanotubes with high activity for oxygen reduction in alkaline media. *Int. J. Hydrogen Energ.* **36,** 2258–2265 (2011).
13. Dai, L. M., Xue, Y. H., Qu, L. T., Choi, H. J. & Baek, J. B. Metal-Free Catalysts for Oxygen Reduction Reaction. *Chem. Rev.* **115,** 4823–4892 (2015).
14. Kwon, K., Sa, Y. J., Cheon, J. Y. & Joo, S. H. Ordered mesoporous carbon nitrides with graphitic frameworks as metal-free, highly durable, methanol-tolerant oxygen reduction catalysts in an acidic medium. *Langmuir* **28,** 991–996 (2012).
15. Li, X. H., Wang, X. & Antonietti, M. Solvent-free and metal-free oxidation of toluene using O$_2$ and g-C$_3$N$_4$ with nanopores: nanostructure boosts the catalytic selectivity. *ACS Catal.* **2,** 2082–2086 (2012).
16. Chen, X. F., Zhang, J. S., Fu, X. Z., Antonietti, M. C. & Wang, X. C. Fe-g-C$_3$N$_4$-catalyzed oxidation of benzene to phenol using hydrogen peroxide and visible light. *J. Am. Chem. Soc.* **131,** 11658–11659 (2009).
17. Katsumata, H., Sakai, T., Suzuki, T. & Kaneco, S. Highly efficient photocatalytic activity of g-C$_3$N$_4$/Ag$_3$PO$_4$ hybrid photocatalysts through Z-scheme photocatalytic mechanism under visible light. *Ind. Eng. Chem. Res.* **53,** 8018–8025 (2014).
18. Kumar, S., Kumar, B., Baruah, A. & Shanker, V. Synthesis of magnetically separable and recyclable g-C$_3$N$_4$-Fe$_3$O$_4$ hybrid nanocomposites with enhanced photocatalytic performance under visible-light irradiation. *J. Phys. Chem. C* **117,** 26135–26143 (2013).
19. Shi, H. F., Chen, G. Q., Zhang, C. L. & Zou, Z. G. Polymeric g-C$_3$N$_4$ coupled with NaNbO$_3$ nanowires toward enhanced photocatalytic reduction of CO$_2$ into renewable fuel. *ACS Catal.* **4,** 3637–3643 (2014).

20. Yao, Y. J. et al. Magnetic $ZnFe_2O_4$-C_3N_4 hybrid for photocatalytic degradation of aqueous organic pollutants by visible light. *Ind. Eng. Chem. Res.* **53,** 17294–17302 (2014).

21. Chen, X. F., Zhang, J. S., Fu, X. Z., Antonietti, M. & Wang, X. C. Fe-g-C_3N_4-catalyzed oxidation of benzene to phenol using hydrogen peroxide and visible light. *J. Am. Chem. Soc.* **131,** 11658–11659 (2009).

22. Wang, X. C., Chen, X. F., Thomas, A., Fu, X. Z. & Antonietti, M. Metal-Containing Carbon Nitride Compounds: A New Functional Organic-Metal Hybrid Material. *Adv. Mater.* **21,** 1609–1612 (2009).

23. Tian, J. Q. et al. Three-Dimensional Porous Supramolecular Architecture from Ultrathin g-C_3N_4 Nanosheets and Reduced Graphene Oxide: Solution Self-Assembly Construction and Application as a Highly Efficient Metal-Free Electrocatalyst for Oxygen Reduction Reaction. *ACS Appl. Mater. Inter.* **6,** 1011–1017 (2014).

24. Liu, Q. & Zhang, J. Graphene supported Co-g-C_3N_4 as a novel metal-macrocyclic electrocatalyst for the oxygen reduction reaction in fuel cells. *Langmuir* **29,** 3821–3828 (2013).

25. Wang, M. Q. et al. Pyrolyzed Fe-N-C composite as an efficient non-precious metal catalyst for oxygen reduction reaction in acidic medium. *ACS Catal.* **4,** 3928–3936 (2014).

26. Zou, X. X. et al. Efficient oxygen evolution reaction catalyzed by low-density Ni-doped Co_3O_4 nanomaterials derived from metal-embedded graphitic C_3N_4. *Chem. Commun.* **49,** 7522–7524 (2013).

27. Wang, Z. L., Xu, D., Xu, J. J. & Zhang, X. B. Oxygen electrocatalysts in metal-air batteries: from aqueous to nonaqueous electrolytes. *Chem. Soc. Rev.* **43,** 7746–7786 (2014).

28. Du, Z. Z. et al. Electrocatalytic performances of $LaNi_{1−x}Mg_xO_3$ perovskite oxides as bi-functional catalysts for lithium air batteries. *J. Power Sources* **265,** 91–96 (2014).

29. Li, S. S., Cong, H. P., Wang, P. & Yu, S. H. Flexible nitrogen-doped graphene/carbon nanotube/Co_3O_4 paper and its oxygen reduction activity. *Nanoscale* **6,** 7534–7541 (2014).

30. Ye, L. Q., Liu, J. Y., Jiang, Z., Peng, T. Y. & Zan, L. Facets coupling of BiOBr-g-C_3N_4 composite photocatalyst for enhanced visible-light-driven photocatalytic activity. *Appl. Catal. B-Environ.* **142,** 1–7 (2013).

31. Mickevičius, S. et al. Investigation of epitaxial $LaNiO_{3−x}$ thin films by high-energy XPS. *J. Alloy. Compd.* **423,** 107–111 (2006).

32. Barr, T. L. An ESCA study of the termination of the passivation of elemental metals. *J. Phys. Chemistry* **82,** 1801–1810 (1978).

33. Liu, Q. C. et al. Artificial Protection Film on Lithium Metal Anode toward Long Cycle-Life Lithium-Oxygen Batteries. *Adv. Mater.* **27,** 5241–5247 (2015).

34. Suntivich, J. et al. Design principles for oxygen-reduction activity on perovskite oxide catalysts for fuel cells and metal-air batteries. *Nat. Chem.* **3,** 546–550 (2011).

35. Niu, W. H. et al. Mesoporous N-Doped Carbons Prepared with Thermally Removable Nanoparticle Templates: An Efficient Electrocatalyst for Oxygen Reduction Reaction. *J. Am. Chem. Soc.* **137,** 5555–5562 (2015).

36. Lin, L., Zhu, Q. & Xu, A. W. Noble-metal-free Fe-N/C catalyst for highly efficient oxygen reduction reaction under both alkaline and acidic conditions. *J. Am. Chem. Soc.* **136,** 11027–11033 (2014).

37. Suntivich, J., May, K. J., Gasteiger, H. A., Goodenough, J. B. & Shao-Horn, Y. A perovskite oxide optimized for oxygen evolution catalysis from molecular orbital principles. *Science* **334,** 1383–1385 (2011).

38. Jin, C., Yang, Z. B., Cao, X. C., Lu, F. L. & Yang, R. Z. A novel bifunctional catalyst of $Ba_{0.9}Co_{0.5}Fe_{0.4}Nb_{0.1}O_{3−δ}$ perovskite for lithium-air battery. *Int. J. of Hydrogen Energ.* **39,** 2526–2530 (2014).

39. Zhao, Y. L. et al. Hierarchical mesoporous perovskite $La_{0.5}Sr_{0.5}CoO_{2.91}$ nanowires with ultrahigh capacity for Li-air batteries. *P. Natl. Acad. Sci.* **109,** 19569–19574 (2012).

40. Zhang, D. W. et al. Active $LaNi_{1−x}Fe_xO_3$ bifunctional catalysts for air cathodes in alkaline media. *J. Mater. Chem. A* **3,** 9421–9426 (2015).

41. Dai, L., Xue, Y., Qu, L., Choi, H. J. & Baek, J. B. Metal-Free Catalysts for Oxygen Reduction Reaction. *Chem. Rev.* **115,** 4823 (2015).

42. Deng, D. H. et al. Toward N-doped graphene via solvothermal synthesis. *Chem. Mater.* **23,** 1188–1193 (2011).

43. Xu, J. J. et al. Synthesis of Perovskite-Based Porous $La_{0.75}Sr_{0.25}MnO_3$ Nanotubes as a Highly Efficient Electrocatalyst for Rechargeable Lithium-Oxygen Batteries. *Angew. Chem. Int. Edit.* **52,** 3887–3890 (2013).

44. Liu, Q. C. et al. Flexible and Foldable Li-O_2 Battery Based on Paper-Ink Cathode. *Adv. Mater.* **27,** 8095–8101 (2015).

Acknowledgements

Author Contributions

D.Z. conceived the project. Y.W. designed the experiments. Y.W. and T.W. performed the experiments, characterization and electrochemical performance test. Y.W., Y.Z., X.H. and S.X. analysed the results. All authors discussed the results and wrote the manuscript. J.S. and D.Z. revised the manuscript.

Additional Information

Competing financial interests: The authors declare no competing financial interests.

How to cite this article: Wu, Y. et al. Electrocatalytic performances of g-C_3N_4-$LaNiO_3$ composite as bi-functional catalysts for lithium-oxygen batteries. *Sci. Rep.* **6,** 24314; doi: 10.1038/srep24314 (2016).